High-temperature crystallization behaviour of amorphous $Fe_{80}B_{20}$

O. T. INAL, L. KELLER
Department of Metallurgical and Materials Engineering, New Mexico Institute of Mining and Technology, Socorro, New Mexico 87801, USA

F. G. YOST
Sandia Laboratories, Albuquerque, New Mexico 87185, USA

Samples of 0.003 in. round $Fe_{80}B_{20}$ amorphous wires were annealed *in vacuo* for 1 sec to 8 h periods at 780° C and the crystallinity induced in these wires from this heat treatment was studied through X-ray diffraction and field-ion microscopy. X-ray diffraction studies indicate that complete crystallinity is produced following 1 sec anneal at 780° C. However, the initial product is a primitive-tetragonal Fe_3B phase unlike the body-centred tetragonal Fe_3B observed in low-temperature isothermal transformation studies with this alloy. The Fe_3B phase is seen to persist in the diffraction patterns for annealing durations of up to 15 min. Upon annealing for periods of up to 1 h, an intermediate three-phase structure consisting of α-Fe, Fe_3B, and Fe_2B is seen to result with a gradual decrease in the Fe_3B phase corresponding to longer annealing durations. Anneals of more than 1 h at 780° C are seen to result in the disappearance of the Fe_3B phase producing a two-phase microstructure consisting of α-Fe (b c c) and Fe_2B (b c t). Field-ion-microscopy with a pure neon imaging gas at 78 K likewise indicates that existence of a three-stage phase structural change during the isothermal anneals, and the atomic arrangement of the various species are quite readily discernible because of the different symmetries contained in the three distinct phases.

1. Introduction

Interest in the amorphous $Fe_{80}B_{20}$ alloy has evolved from the fact that it possesses the enhanced mechanical, magnetic, electrical and chemical properties generally attributed to amorphous materials as well as the fact that this alloy is found to be the strongest, hardest and stiffest metallic glass evaluated to date. The fact that it contains only one metalloid, boron, is also seen to lead to greater thermal stability in this amorphous alloy [1].

The uses expected of metallic glasses in general are dependent on not only the thermal stability they possess but also on their crystallization behaviour which heat treatment or exposure to high temperature may introduce. A thorough understanding, therefore, of the kinetics of crystallization in metallic glasses could lead to improved

design as well as to possible production of phases or phase mixtures suitable for a given engineering application. For this reason, both direct heating and isothermal annealing studies have been made on amorphous alloys to elucidate nucleation and growth mechanisms of crystalline phases in these media. For example, X-ray analyses following heat treatments of (Fe, Ni, Cr) metal and (B, P) metalloid containing metallic glasses show that, either direct heating or isothermal annealing of these amorphous alloys lead to a crystalline phase with a $(Fe, Ni, Cr)_3(B, P)$ type of crystal structure having either a body-centred-tetragonal cell [2–7] or an orthorhombic [8] symmetry. These studies are summarized, with the relevant X-ray evaluated lattice constants, in Table I.

The purpose of this experiment was to evaluate

T A B L E I X-ray diffraction analyses on crystallization behaviour of $(Fe, Ni, Cr)_3 (B, P)$ type amorphous alloys.

Reference	Alloy	Heat treatment	$(Fe, Ni, Cr)_3 (B, P)$ structure type	Cell
[2]	$Fe_{80}B_{20}$ $Fe_{50}Ni_{30}B_{20}$	2 h, 380° C	$a_0 = 8.63$ Å $c_0 = 4.29$ Å	b c t
[3]	$Fe_{32}Ni_{36}Cr_{14}P_{12}B_6$	500° C	$a_0 = 8.95$ Å $c_0 = 4.39$ Å	
[4]	$Fe_{85}B_{15}$ $Fe_{84}B_{16}$ $Fe_{73}Cr_{10}B_{17}$	477° C	$a_0 = 8.63$ Å $c_0 = 4.37$ Å	b c t
[5]	$Ni_x P_y$	600° C	$a_0 = 8.93$ Å $c_0 = 4.39$ Å	b c t
[6]	$Ni_{40}Fe_{40}P_{14}B_6$	2 h, 370° C	$a_0 = 8.90$ Å $c_0 = 4.39$ Å	b c t
[7]	$Fe_{32}Ni_{36}Cr_{14}P_{12}B_6$	400° C	$a_0 = 8.85$ Å $c_0 = 4.38$ Å	b c t
		600° C	$a_0 = 9.00$ Å $c_0 = 4.49$ Å	b c t
[8]	$Fe_{40}Ni_{40}B_{20}$	500° C	$a_0 = 4.437$ Å $b_0 = 5.340$ Å $c_0 = 6.638$ Å	Orthorhombic
Present work	$Fe_{80}B_{20}$	1 sec – 15 min 780° C	$a_0 = 8.623$ Å $c_0 = 4.294$ Å	Primitive tetragonal

changes in the atomic structure and elucidate nucleation and growth characteristics of the crystalline phase or phases in an $Fe_{80}B_{20}$ metallic glass. For this purpose heat treatments at 780° C, for periods from 1 sec to 8 h, were made on melt-extracted [9] amorphous wire samples and evaluations were done through X-ray diffraction analyses and field-ion microscopy. This temperature of heat treatment is higher than any of the previously mentioned studies and is exactly twice that of the recorded crystallization temperature, of 390° C [1], for this material.

2. Procedure

Annealing treatments given to the amorphous $Fe_{80}B_{20}$ wires were made in a high-vacuum (2 × 10^{-7} Torr) chamber utilizing resistive heating. Following heat treatment, X-ray diffraction evaluation followed by etching and imaging in the field-ion microscope were made on the wire samples.

2.1. X-ray diffraction analyses

Debye—Scherrer powder diffraction technique was used to analyse the amorphous and heat-treated wires with filtered FeK_α radiation (40 kV 20 mA) with a camera diameter of 57.3 mm and an exposure time of 4 h.

2.2. Field-ion microscopy

Field-ion microscope analyses of the samples were made at 78 K in a medium of pure neon gas with continuous titanium gettering to insure image cleanliness. The design feature of this microscope are given elsewhere [10].

Field-emission end forms used in these analyses were produced through electroetching of the wires in a solution of 20 vol% HNO_3, 20 vol% HCl and 60 vol% methanol (CH_3OH) at 1 to 3 V a.c. Following electroetching, samples were placed in the field-ion microscope and the system evacuated to 1×10^{-8} Torr. Imaging, following cooling of the sample to 78 K, was made in a background of 5×10^{-5} Torr neon gas.

3. Experimental results

Amorphous $Fe_{80}B_{20}$ wires were heat treated at 780° C for periods of 1, 5, 15, 30 and 45 sec, 1, 15, 22.5 and 30 min, 1, 2.25, 4, 6 and 8 h. X-ray diffraction analyses followed by field-ion microscope characterization of the annealed microstructures were then made.

3.1. X-ray diffraction

Debye—Scherrer powder diffraction results are listed in Table I, for annealing periods of 1 sec to 15 min, with lattice constants of the predominant

Fe$_3$B phase. The refinement procedure [14] followed to achieve $a_0 = 8.623 \pm 0.005$ Å and $c_0 = 4.294 \pm 0.005$ Å values (following the procedure in the analyses by Rundqvist for Fe$_3$B [12]) as the lattice constants for this primitive tetragonal lattice are tabulated and included in Table AI of the Appendix.

X-ray analyses show that the isothermal annealing at 780° C of an amorphous Fe$_{80}$B$_{20}$ wire is characterized by two phase transformations. The first transformation occurs after an annealing time of 1 sec when the Fe$_3$B phase is seen to crystallize from the previous fully amorphous state. After heat treatment of 1 h the Fe$_3$B phase is entirely transformed into a body-centred cubic

α-Fe and a body-centred tetragonal Fe$_3$B phase. Intermediate stages, where all three phases are present, are seen to exist in the range of 15 min to 1 h annealing time. Further increased time at temperature, up to 8 h, was not seen to yield much difference in the crystal and microstructure of the two-phase mixture in the X-ray analyses.

Table II lists the annealing times at 780° C with the corresponding phases and Bravais lattices observed in the X-ray analyses. X-ray diffraction patterns of unique changes observed in the crystal structure are shown in Fig. 1 for an amorphous sample (Fig. 1a), after 30 sec anneal (Fig. 1b), following 1 h heat treatment (Fig. 1c) and after 2.25 h at 780° C (Fig. 1d).

T A B L E II X-ray diffraction and FIM analyses of the crystallization products of Fe$_{80}$B$_{20}$ during isothermal annealing at 780° C

| Annealing time	X-ray diff. analyses	Cell	FIM observations
—	amorphous halo	—	no long-range order; random distribution of atoms
1 sec	Fe$_3$B	Primitive tetragonal	Small patches of α-Fe; partial ring structure of Fe$_3$B
5 sec	Fe$_3$B	p t	large and small α-Fe precipitates in an Fe$_3$B matrix
15 sec	Fe$_3$B	p t	Small Fe islands in Fe$_3$B matrix
30 sec	Fe$_3$B	p t	Small crystalline α-Fe in a matrix of Fe$_3$B
45 sec	Fe$_3$B	p t	α-Fe twin packet in Fe$_3$B matrix
1 min	Fe$_3$B	p t	More α-Fe twins in Fe$_3$B matrix
15 min	Fe$_3$B	p t	α-Fe in a matrix of Fe$_3$B and first appearance of Fe$_2$B
22.5 min	Fe$_3$B Fe$_2$B α-Fe	p t b c t b c c	α-Fe iron islands and more ordered (with poles) Fe$_2$B
30 min	Fe$_3$B Fe$_2$B α-Fe	p t b c t	Large Fe$_2$B islands with α-Fe on the edges
1 h	Fe$_3$B Fe$_2$B α-Fe	p t b c t b c c	Only Fe$_2$B and α-Fe showing at the exposed area
2.25 h	Fe$_2$B α-Fe	b c t b c c	Large islands of Fe$_2$B and α-Fe
4 h	Fe$_2$B α-Fe	b c t b c c	α-Fe hemisphere and Fe$_2$B separated by a phase boundary
6 h	Fe$_2$B α-Fe	b c t b c c	Phases are large enough to cover imaging area individually
8h	Fe$_2$B α-Fe	b c t b c c	Phases are large enough to cover imaging area individually
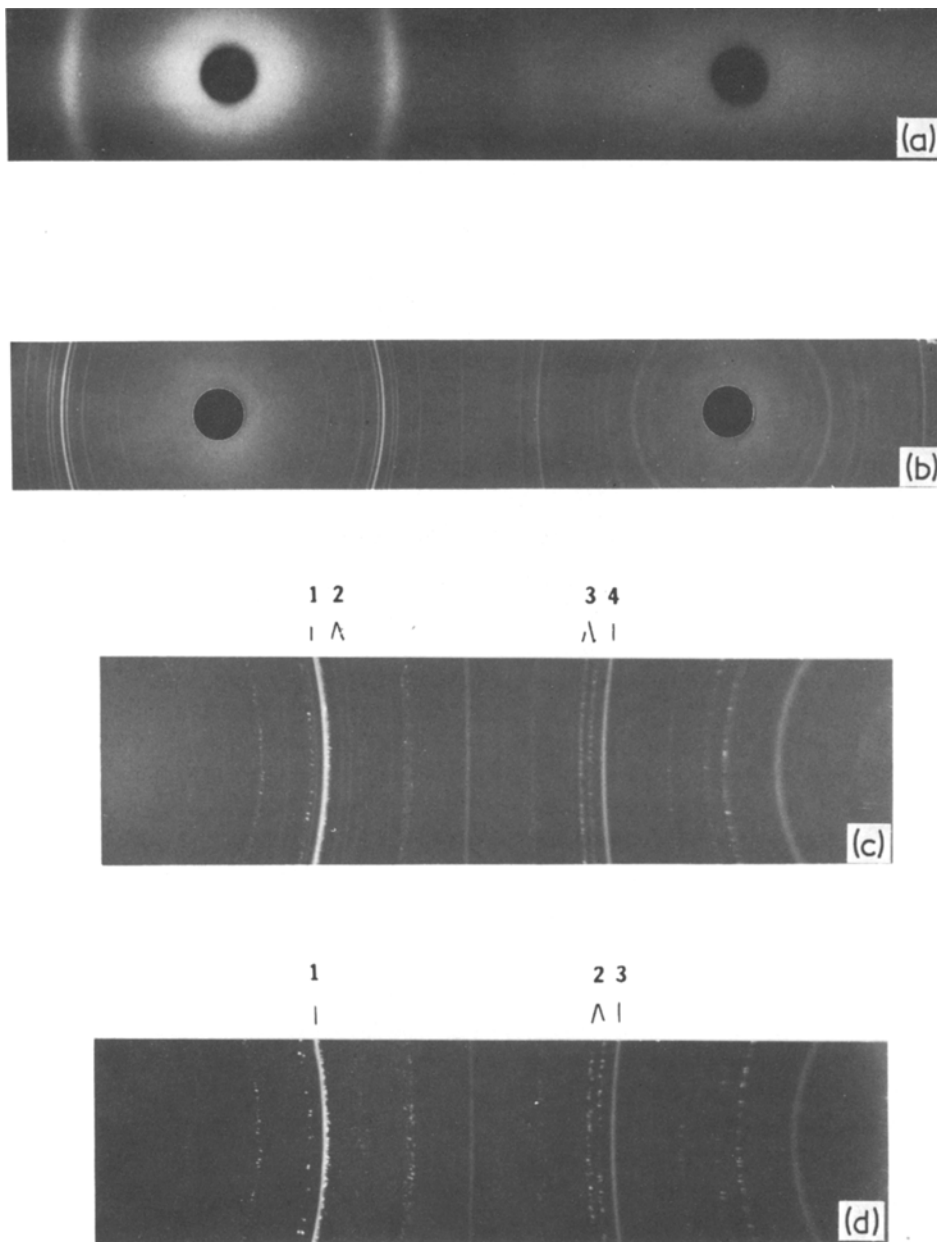
Figure 1 Debye–Scherrer powder diffraction patterns; (a) amorphous (untreated) $Fe_{80}B_{20}$; (b) pattern following 30 sec anneal with only Fe_3B phase present; (c) pattern following 1 h heat treatment with Fe_3B, Fe_2B and α-Fe phase present in the enlarged photograph: From left to right: (1) $Fe_3B_{(330)}$ + $Fe_2B_{(121)}$ + α-$Fe_{(110)}$; (2) $Fe_3B_{(420)}$ + $Fe_3B_{(411)}$; (3) $Fe_2B_{(330)}$ + $Fe_2B_{(141)}$; and (4) α-$Fe_{(211)}$. (d) Pattern following 2.25 h heat treatment with Fe_2B and α-Fe phases present in this enlarged photograph. From left to right: (1) $Fe_2B_{(121)}$ + α-$Fe_{(110)}$; (2) $Fe_2B_{(330)}$ + $Fe_2B_{(141)}$; (3) α-$Fe_{(211)}$.

3.2. Field-ion microscopy

Field-ion microscopy observations of microstructures present as a function of heat-treatment time at $780°$ C are also summarized in Table II and shown in Fig. 2 to 14.

Fig. 2 shows the initial amorphous atomic arrangement with random atomic distribution and no obvious indication of symmetry relating to long range atomic order. Fig. 3 shows the sample following 1 sec heat treatment consisting of small precipitates of Fe comprised of 3 to 5 atom clusters brighter that the matrix Fe_3B. The latter is seen
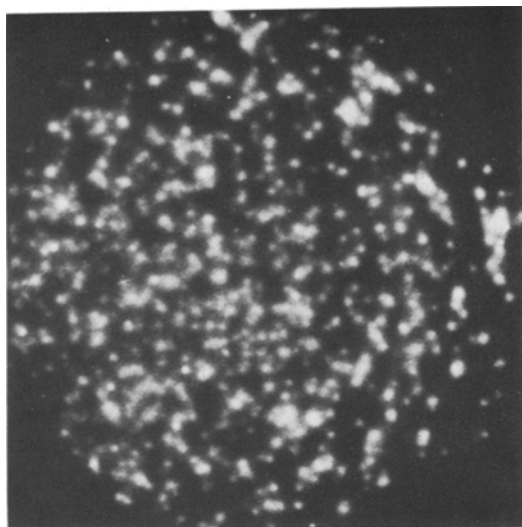
Figure 2 Field-ion micrograph of the amorphous $Fe_{80}B_{20}$ alloy showing random atomic distribution.

to exhibit partial ring structure but not the symmetry of a densely packed atomic arrangement. A field-evaporation sequence of four atomic layers is shown in Fig. 4 portraying the microstructure attained following 5 sec anneal at 780° C. Large precipitates of Fe are seen as dark areas in these micrographs indicating the difference in the best image voltages of the matrix Fe_3B and the large Fe crystals. However, small clusters of Fe, consisting of a few atoms each are imaged at the same voltages as the Fe_3B matrix. Heat treatment of 15 sec is seen, Fig. 5, to yield small crystallites of Fe in a
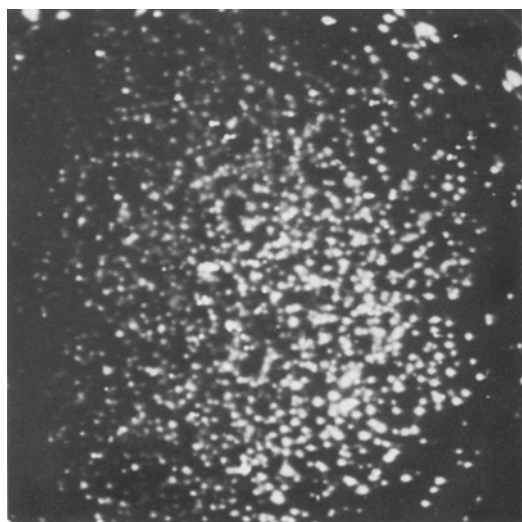

Figure 3 Micrograph of a sample annealed for 1 sec at 780° C showing partial ring formation and small clusters of iron.

matrix of Fe_3B with no indication of the large Fe precipitates coalescing into islands large enough to encompass the entire imaging area. Fig. 6 shows the microstructure following 30 sec heat treatment and consists of small clusters of Fe in a matrix of Fe_3B phase. Following 45 sec anneal, shown in Fig. 7, the microstructure is seen to exhibit an Fe twin packet in the Fe_3B matrix. The twinned structure of α-Fe is also seen in Fig. 8 following 1 min of heat treatment of 780° C. Fig. 9 shows a field-evaporation sequence through the sample annealed for 15 min and the existence of a three-phase mixture. This microstructure consist of Fe, Fe_2B and the matrix Fe_3B phase and is quite clear from the imaging differences exhibited by the phases. α-Fe is seen as much brighter atoms coalesced together, Fe_2B phase exhibits poles and a suggestion of symmetry while the Fe_3B phase is seen to lack symmetry and consists of random atomic arrangement. Amorphous wire annealed for 22.5 min, shown in Fig. 10, is seen to consist of bright Fe islands surrounding the Fe_2B phase the latter being recognizable by the prominent poles. The fact that the Fe_3B phase is not apparent in these micrographs indicates that the two product phases have grown to be large enough to occupy the whole imaging area. Fig. 11 shows the sample following 30 min of annealing in a field evaporation sequence. The Fe_2B phase, with numerous poles, is seen to have α-Fe islands at the very edges. Again, the large dimensions of the product phases does not seem to allow for the Fe_3B component to be present in the imaging area. Annealing for a period if 1 h also shows only the α-Fe and Fe_2B product phases to be present as shown in Fig. 12. The phase boundary observed quite clearly distinguishes the very top and bottom, densely populated, bright image of α-Fe from the Fe_2B phase domain with its sparsely populated Fe spots in the image. Fig 13 shows micrographs of a sample annealed for 2.25 h. Here, it is seen that growth of product phases has been extensive enough for each to occupy the whole imaging area; Fig. 13a and b are those of α-Fe regions while Fig. 13c and d portray the Fe_2B phase. Finally, Fig 14 is seen to contain an almost complete hemisphere of b c c iron crystal, a phase boundary and the Fe_2B phase at the bottom portion of the micrograph.

Longer anneals, of up to 8 h, were seen to lead to images of single phase regions of either α-Fe or Fe_2B and were very distinctly weaker under field-
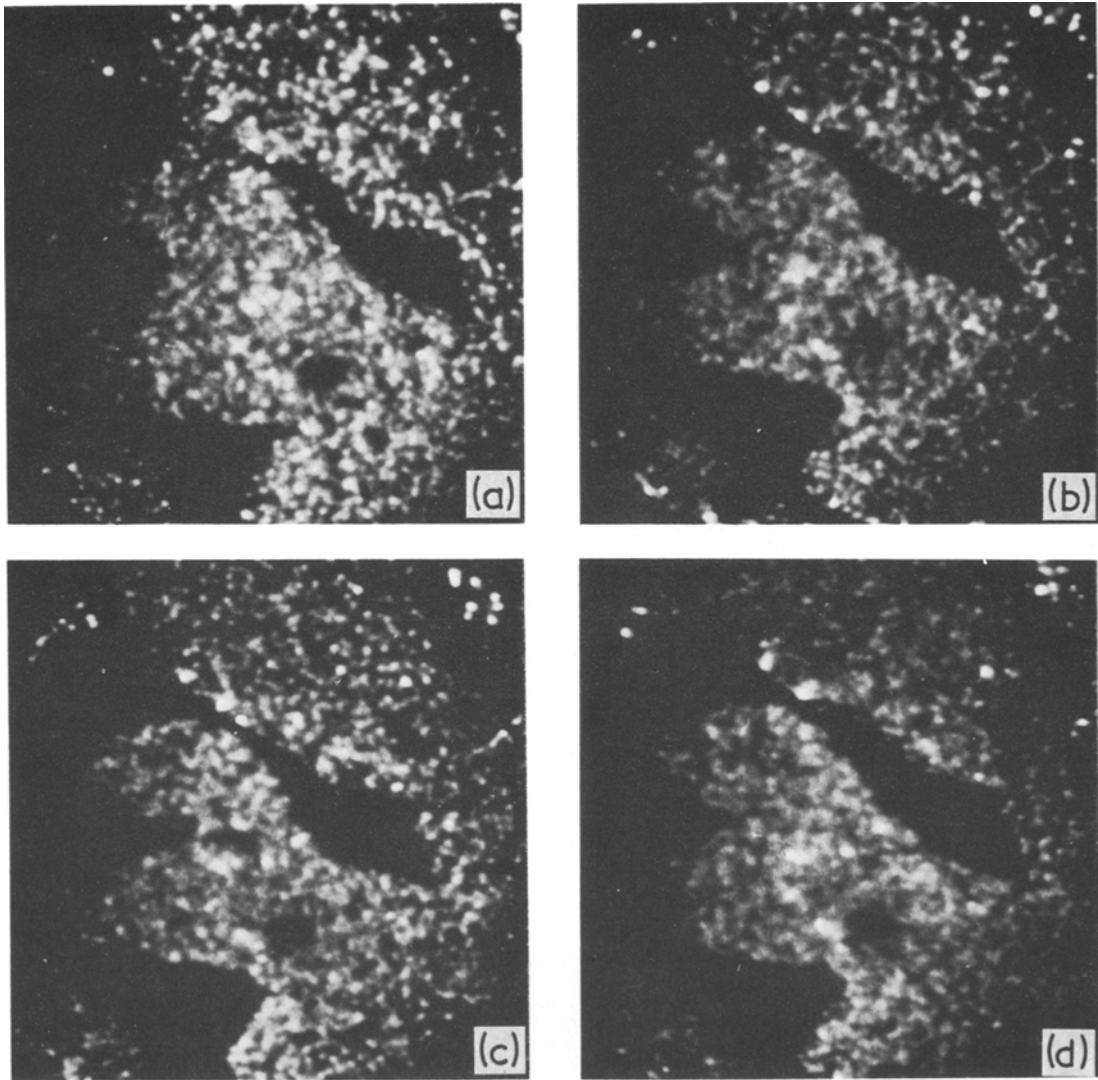
Figure 4 Sample following 5 sec anneal; large, geometrically shaped precipitates in the matrix and small clusters of iron in the Fe_3B matrix are shown.

induced stresses of imaging in the field-ion microscope. Since no uniquely different phase structures were observed in these latter heat treatments, they will not be further discussed in this article.

4. Discussion

The results of this study indicate that parallel X-ray diffraction analyses and field-ion microscopy are indeed quite compatible and necessary for such a study involving three different stages of phase changes. In transforming from a fully amorphous matrix to the eventual appearance and growth of the final two-phase mixture the nature, size and distribution of the intermediate phases could only be evaluated with data from both

analyses. For example, in the early stages of the isothermal anneal (1 sec to 15 min at 780° C) it is seen that the presence of finely distributed pure iron crystals are not clearly indicated in the X-ray diffraction patterns while in longer durations of anneal (1 h to 4 h) the individual phases are developed to such large dimensions that the field-ion microscope is able to image only portions of the actual microstructures present. Whereas the field-ion analyses show the exact atomic configuration present in each phase, information from X-ray diffraction data is needed to help not only characterize structure but also lead to educated assumptions with regards to lattice constant values and grain dimensions.
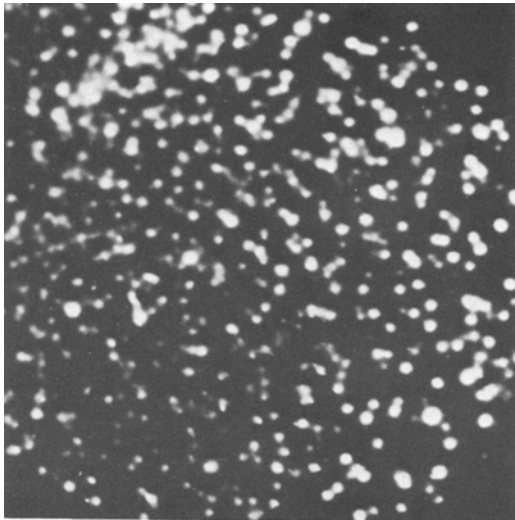
Figure 5 Micrograph of the $Fe_{80}B_{20}$ wire following 15 sec heat treatment at 780° C showing small clusters of iron on the upper left-hand corner and the Fe_3B matrix.
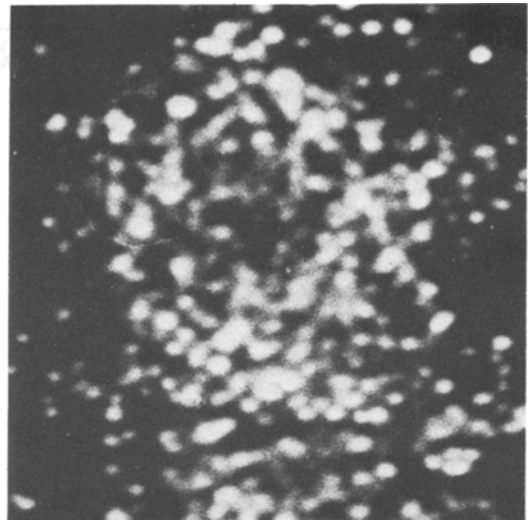
4.1. X-ray diffraction analysis

The Fe_3B matrix phase, the first crystallized product of $Fe_{80}B_{20}$ upon annealing, belongs to the tetragonal crystal system having a primitive cell. The space group is seen to be $P4_{2/n}$ with the allowable reflection conditions $hk0 : h + k = 2n$ and $00l : l = 2n$ [11]. The calculated intensities (calculations were based on the atomic positions of Fe and B given by Rundqvist [12]) are in reasonably good agreement with the observed intensities of the powder diffraction lines shown

Figure 7 Following 45 sec anneal sample shows a twin packet, twinning plane at approximately 30° to the horizontal, consisting of iron atoms.

in the refinement computation included in Appendix 1. The presence of pure Fe nuclei along with the Fe_3B phase, at this initial stage, is not quite clear from the diffraction patterns although a strong suggestion of this is that the observed intensity, with $d_{330} = 2.032$ Å, is unusually high (strongest α-Fe line is $d_{110} = 2.024$ Å).

When the transformation is completed to a phase mixture consisting of the Fe_2B and α-Fe phases the corresponding diffraction patterns are easily discernible as shown in Fig. 1d. While α-Fe
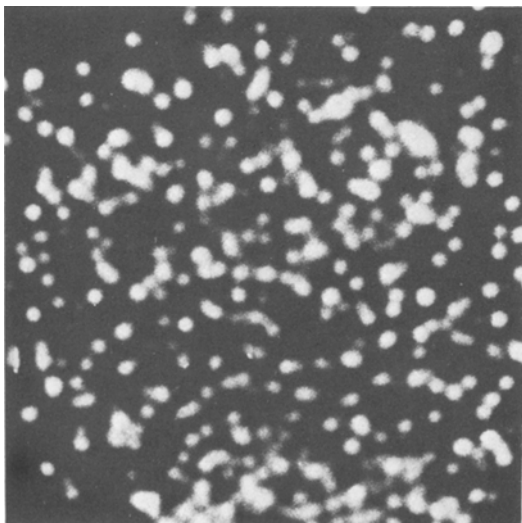

Figure 6 Sample following 30 sec anneal at 780° C showing small clumps of iron in a matrix of Fe_3B.
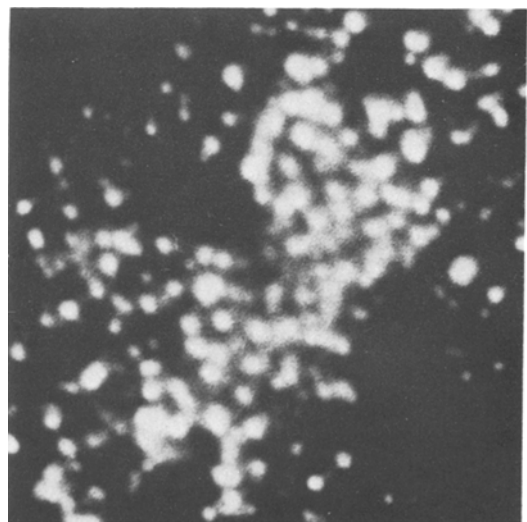

Figure 8 1 min annealing is seen to introduce a twin packet, at approximately 120° to the horizontal, consisting of iron atoms.
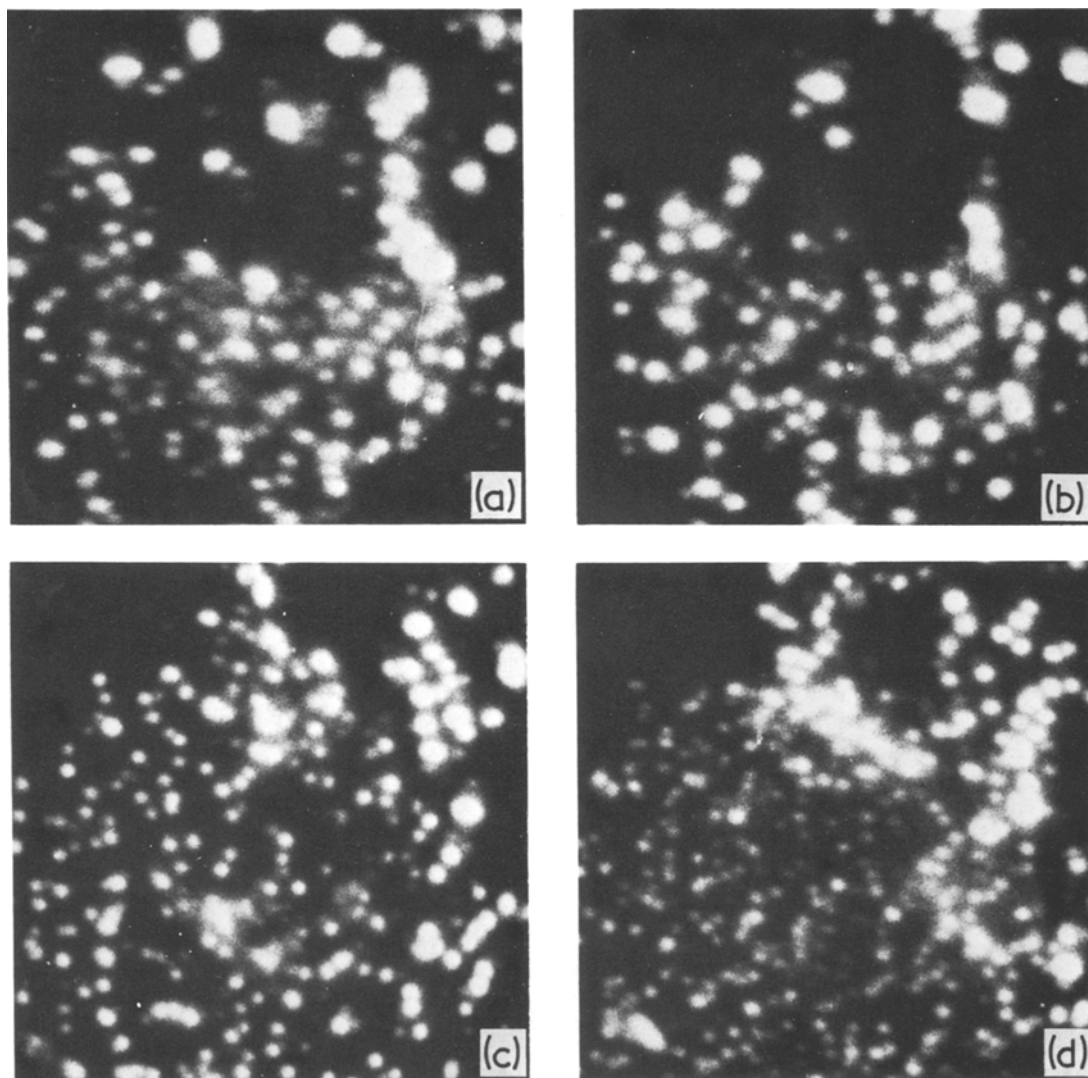
1953

Figure 9 Field-evaporation sequence through a sample annealed for 15 min. The micrographs are characterized by clumps of pure iron in the middle separating the Fe_3B zone (lower portion) from the Fe_2B phase domain (upper portion).

is seen to produce smooth diffraction lines with uniform blackening, the lines that correspond to Fe_2B consist of single spots. This indicates that the α-Fe phase consists of uniformly distributed small crystallites whereas the Fe_2B grains are larger in size and the percentage of Fe_2B phase present seems to be less compared to the α-Fe phase. Since there is no obvious line broadening, it can be concluded that the crystallite sizes of both phases are greater than 1000 Å·

4.2. Field-ion microscopy

Field-ion microscopy has achieved only limited success in imaging concentrated alloys because of

the differences introduced in the electronic configuration of the imaging surface by the differences in size and electro-negativity of the species present in the alloy [13]. Since the size and the chemical valence of iron and boron are considerably different it was not surprising to find only Fe image spots to be visible in the images of Fe_2B and Fe_3B, possibly suggesting an insufficient field ionization above boron atoms on the imaging surface. The image features of pure iron were also seen to be considerably altered when alloyed with boron, again suggesting that the charge transfer between the two species resulted in a change of field-ionization features above these phases [13].
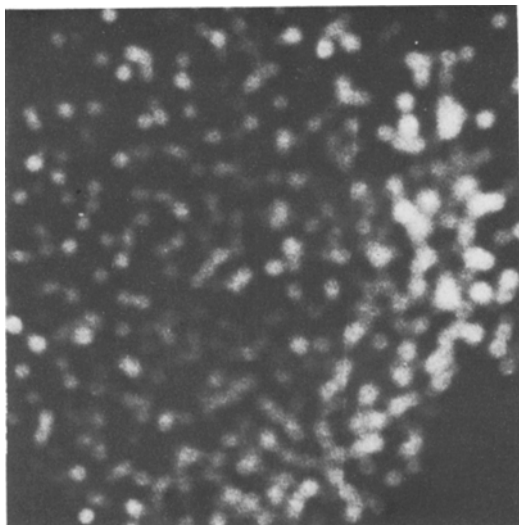
Figure 10 Micrographs showing pure iron clusters to the right, and Fe_2B phase.

Pure iron image spots were seen to be much brighter and clearly defined in the image and were of larger dimensions than iron spots observed in the Fe_2B and Fe_3B phases. Field evaporation features were also seen to be quite different in the various phases imaged. Whereas pure iron domains were seen to field evaporate in single-atom fashion, iron alloyed with boron, Fe_2B and Fe_3B, was seen to evaporate with sudden wave-like motion, Therefore, it was easily possible to discern pure iron from the alloyed iron phases in the field-ion images.

To distinguish between the two alloy phases, the following points were considered: (a) the initially crystallized alloy phase was seen to contain only partial rings and no obvious symmetry while the phase developed following 1 h heat treatment, along with pure iron domains, exhibited poles and a suggestion of a lattice symmetry; (b) the former phase, in the micrographs, seemed to contain more iron spots than the iron population of the latter phase, when observed in the same micrographs. Since the X-ray analyses indicate the initial phase as Fe_3B with a primitive tetragonal lattice and a greater population of iron atoms (3:1) it is consistent to see a disordered array of atoms for this phase in comparison to the sparser (with 2:1 ratio) but more symmetric images of the body-centred tetragonal Fe_3B phase.

4.3. Discussion of results

The phase changes observed in this isothermal heat treatment of $Fe_{80}B_{20}$ alloy can be divided into three sections comprised of: (a) the initial transformation of the amorphous alloy into crystalline Fe_3B and α-Fe phases during the period of 1 sec to 15 min annealing; (b) a phase change where Fe_3B is seen gradually to dissociate into Fe_2B and an α-Fe phases within annealing periods of 15 min to 1 h; and (c) structural change involving the disappearance of the Fe_3B phase and a structure consitsting of α-Fe crystallites with larger grained but of smaller proportion Fe_2B phase attained through anneals of longer than 1 h periods. These three stages will be discussed separately.

4.3.1. Initial transformation

During the initial stage of transformation, X-ray analyses consistently show the presence of fully crystalline Fe_3B phase with a primitive tetragonal cell for heat treatments of from 1 sec to 15 min. This is uniquely different from earlier studies with (Fe, Ni, Cr) metal and a (B, P) metalloid systems where the initial crystallization product is observed to pertain to be of either a body-centred tetragonal [2–7] or of an orthorhombic symmetry [8]. This suggests that the Fe_3B matrix phase of the $Fe_{80}B_{20}$ alloy undergoes a slight symmetry change when annealed high above the crystallization temperature.

The presence of an α-Fe constituent in the initial transformation stage is not quite obvious from X-ray observations although evidence of its presence is definitely clear in the field-ion microscope evaluations. For example, in Fig. 3, the small clusters (of 3 to 5 atoms each) of bright-image spots belong to the α-Fe phase. Following 5 sec annealing most of these small clusters are seen to have coalesced and precipitated out of the matrix as indicated by the geometrically shaped dark areas seen in Fig. 4a to d. During field evaporation of these surfaces, atomic evaporation was clearly discernible in these dark areas and only at the best image voltage of the matrix were they seen to exhibit no image spots. The fact that the boundaries between the two phases are so sharply defined indicates that both phases are fully crystalline. The presence of α-Fe in longer annealing duration studies, up to 15 min (shown in Fig. 5 to 9), is indicated by small clusters of this species distributed in the matrix, possibly suggesting the complete dissociation of the larger precipitates from the matrix phase. Another important development within this stage of transformation is the twin packets shown in Fig. 7 and 8, cor-
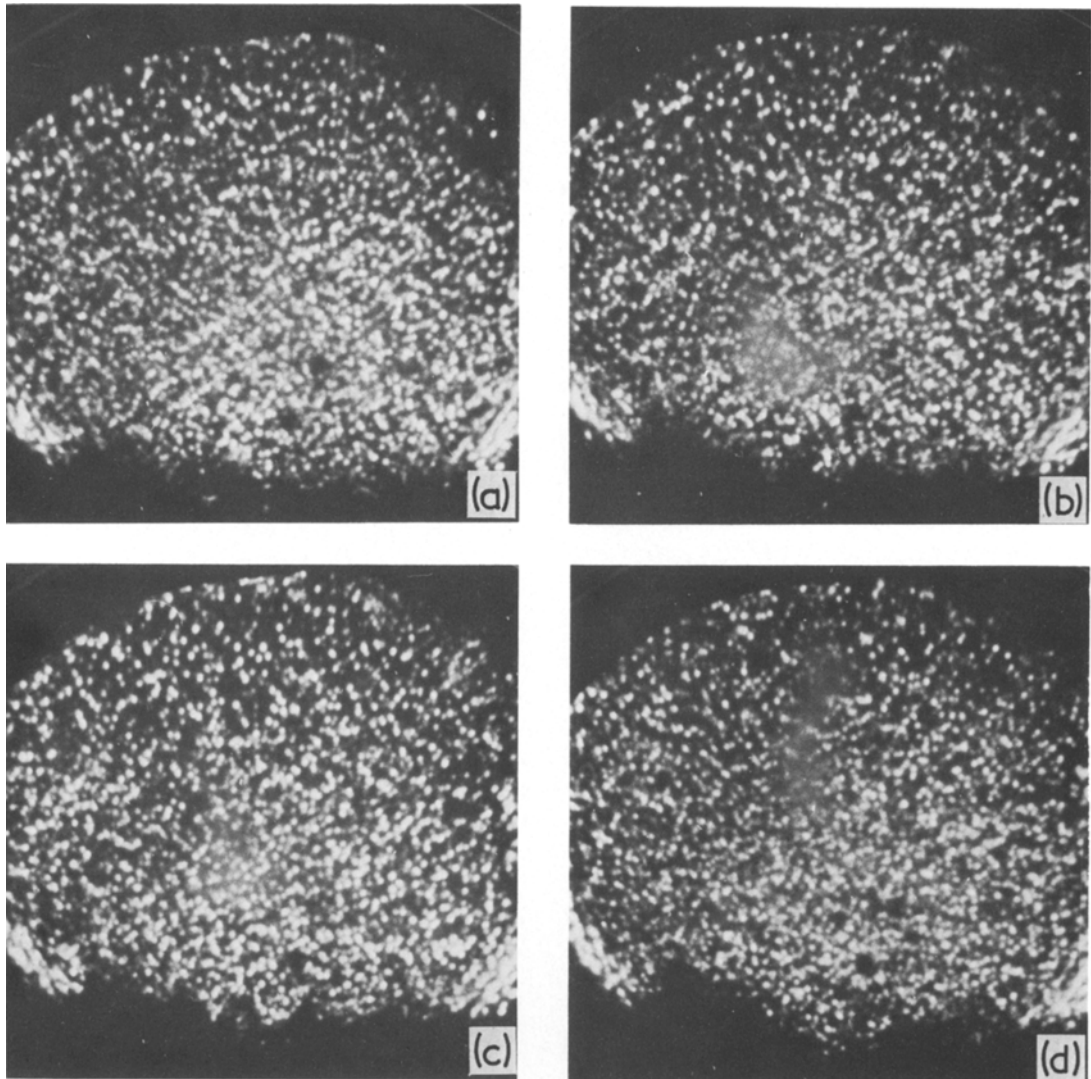
Figure 11 Following 30 min heat treatment, the field evaporation sequence shows the Fe_2B phase with small pure iron clusters and larger clumps at the lower edges.

responding to the 45 sec and 1 min annealing periods, respectively. The twin packets are seen to consist of α-iron atoms in these micrographs.

Appearance of twinning in the product crystalline phases has been observed previously in the analysis of crystallization behaviour of $Fe_{80}B_{20}$ alloy [2]. Upon annealing for 2 h at 380° C, α-Fe was seen in this study to appear as clumps with a definite preferred orientation relationship to the Fe_3B matrix phase. The twinning observed, in this low-temperature heat treatment, is seen to be on $\{2\ 1\ 1\}$ planes of Fe_3B and the twins are seen to divide the microstructure into quadrants. The main difference in these two studies is that the

whole structure is fully crystalline in our case while the Fe_3B matrix phase is bounded by amorphous material in the low-temperature study. Since the lack of symmetry in the field-ion micrographs does not allow for accurate indexing in this study, determining the orientation of the twinning plane is impossible. However, from the size of image spots and the clustering they exhibit, it is quite certain that the two packets consist of iron atoms.

The presence of a pure iron phase in this initial stage of transformation is, of course, consistent with the fact that the matrix of $Fe_{80}B_{20}$ alloy contains more iron atoms than can be accounted for by the Fe_3B phase.
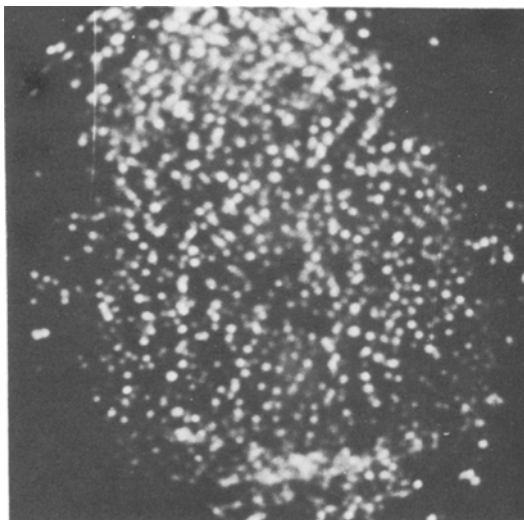
Figure 12 Sample annealed for a period of 1 h exhibiting a microstructure consisting of pure iron clumps at the top and bottom portions of the micrographs with a large domain of Fe_2B phase is the middle.

4.3.2. Intermediate stage

Although X-ray analyses show the first indication of a microstructure consisting of a mixture of three phases following heat treatment of 22.5 min, the field-ion micrographs of 15 min anneal show a strong indication. In Fig. 9a to d, a lower portion of disordered Fe_3B phase is separated from the more symmetric Fe_2B phase by a bright domain consisting of pure iron clusters. On the other hand, while X-ray analyses consistently indicate a microstructure consisting of three phases up to annealing periods of 1 h, the field-ion micrographs are seen to contain only a mixture of Fe_2B and α-Fe phases. This latter fact suggests that the individual phases have already assumed large enough dimensions to cover most of the imaging area and, therefore, there is an overmagnification in essence avoiding the portrayal of the true microstructure of all phases present. For example, Fig. 9 to 12 all show the existence of an Fe_2B phase, with prominent poles and more symmetry than exhibited by the Fe_3B observed in the shorter annealing periods, with clumps of pure iron scattered around in the overall microstructure.

This phase mixture of three microconstituents has not been seen before in the previous heat-treatment studies mentioned earlier and is believed to be a feature of the high annealing temperature utilized in the present study.

4.3.3. Equilibrium stage

Information from X-ray analyses indicate that the Fe_3B matrix phase has completely dissociated into Fe_2B and α-Fe phase following 2.25 h annealing at 780° C, as shown in Fig. 1d. This is strongly supported by the field-ion micrographs of these samples, shown in Fig. 13, where alternate sets of micrographs show either the α-Fe phase (Fig. 13a and b) or the Fe_2B phase (Fig. 13c and d) thus exhibiting the atomic arrangement of the phase that constitutes the tip cap of a given field-ion microscope analysis. Also, the image of a sample following 4 h heat treatment, shown in Fig. 14, exhibits a large grain of α-Fe with a small domain (in the lower left-hand portion of the micrograph) of Fe_2B separated by a poorly defined phase boundary. It is quite obvious that the individual phase dimensions have become large enough to constitute the whole imaging area of the tip cap.

No further phase changes were seen to take place in this stage of heat treatment and the only result, for up to 8 h annealing, was continued growth of the two phases.

As the grains of each species grew, the difficulty of field-ion imaging also increased considerably. The phase boundaries generated were seen to be too weak to withstand the field-induced stresses of imaging, and the fracturing that followed consistently resulted in images of either the α-Fe on the Fe_2B phase.

This stage of heat-treatment behaviour is considerably different from previous work in that the Fe_2B with its body-centred tetragonal cell has not been observed in other studies and, with the α-Fe phase, it seems to constitute the equlibrium product in the transformation of amorphous $Fe_{80}B_{20}$ alloy at 780° C.

5. Conclusions

The conclusions derived from this study include:

(1) heat treatment of the amorphous $Fe_{80}B_{20}$ alloys leads to a three-stage phase transformation with uniquely distinct phase mixtures constituting the microstructure at each stage;

(2) equilibrium phases that emanate from annealing at 780° C are the Fe_2B (b c t) and α-Fe (b c c) phases;

(3) no discernible incubation period exists in the transformation at 780° C and even a heat treatment of 1 sec yields a metastable but totally crystalline Fe_3B matrix phase along with α-Fe;
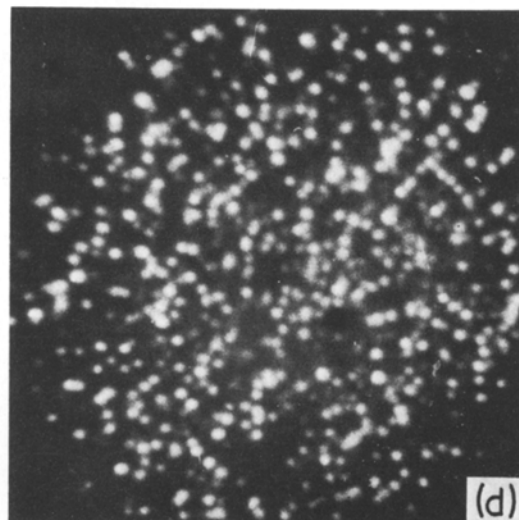
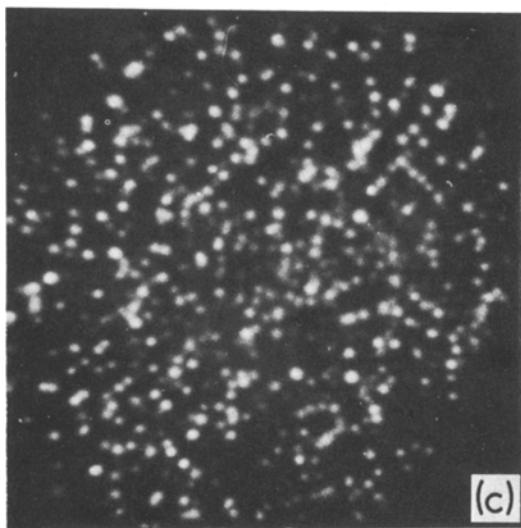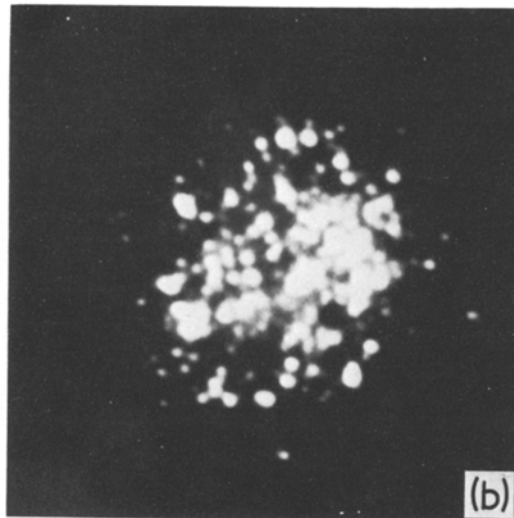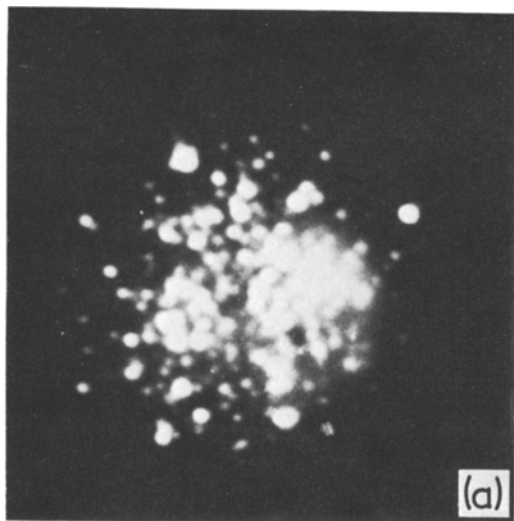(4) information from FIM analyses is invaluable

Figure 13 Sample heat treated for 2.25 h indicating that each phase domain is large enough to image separately; field evaporation sequence through pure iron (a and b) and Fe_2B zone (c and d) are shown in these micrographs.
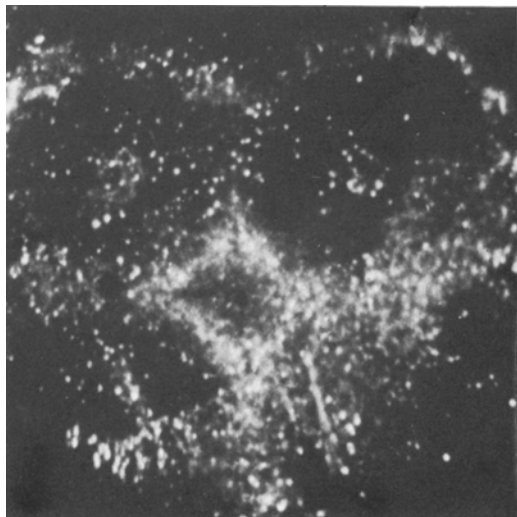

Figure 14 Following 4 h heat treatment the sample exhibits a large hemisphere of iron with a small domain, on the lower left corner, of Fe_2B phase.

at shorter periods of heat treatment at this temperature but, as grain growth takes place, a true picture of overall structure is not possible because of overmagnification. Thus, both techniques, X-ray diffraction and field-ion microscope, are useful methods of analysis for studying phase transformations in amorphous alloys.

Appendix

Acknowledgement

TABLE AI Powder diffraction data of Fe_3B: $a_0 = 8.623$ Å; $c_0 = 4.294$ Å

$h\,k\,l$	d_{obs} Å	Δd_{obs} Å	d_{calc} Å	I^*_{obs}	I^+_{calc}
2 2 0	3.06	0.02	3.05	15	35.8
2 0 1					
2 1 1	2.87	0.01	2.87	5	5.4
3 1 0	2.73	0.01	2.73	10	9.1
2 2 1	2.49	0.01	2.49	5	7.6
3 0 1	2.39	0.01	2.39	10	22.1
3 1 1	2.300	0.009	2.302	30	113.3
0 0 2			2.147		
4 0 0	2.152	0.007	2.155	10	35.7
3 2 1	2.090	0.007	2.089	65	379.5
3 3 0	2.033	0.007	2.032	100	285.0
1 1 2			2.025		
4 2 0	1.931	0.006	1.928	40	188.3
4 0 1			1.926		
4 1 1	1.882	0.005	1.880	50	280.7
2 1 2			1.875		
3 3 1	1.838	0.005	1.837	5	17.6
4 2 1	1.762	0.005	1.759		104.8
2 2 2			1.775	20	
3 0 2	1.720	0.004	1.720	5	9.5
5 1 0	1.690	0.004	1.691		
3 1 2			1.681	30	196.2
5 0 1	1.605	0.004	1.601	5	11.67
4 3 1			1.600		
5 1 1	1.578	0.004	1.573	5	27.4
4 4 0	1.526	0.003	1.524	5	6.3
6 0 0	1.437	0.003	1.437		
4 4 1			1.434	5	5.9
4 4 2			1.435		
6 2 0	1.363	0.003	1.363	20	38.9
6 0 1			1.363		
6 1 1	1.384	0.002	1.364	10	100.1
4 3 2			1.345		
5 1 2	1.330	0.002	1.329	5	21.8
6 2 1	1.299	0.002	1.299	5	20.1
5 2 2	1.281	0.002	1.283	5	13.9
3 0 3			1.281		

h k l	d_{obs} Å	Δd_{obs} Å	d_{calc} Å	I^*_{obs}	$I^\dagger_{calc}$
3 1 3	1.268	0.002	1.267	5	33.5
4 4 2	1.234	0.002	1.234	5	41.1
6 3 1	1.230	0.002	1.231	20	200.5
2 3 2			1.229		
5 5 0	1.218	0.002	1.219		
7 1 0			1.218	30	
5 3 2			1.218		318.4
6 4 0	1.195	0.002	1.196		
6 0 2			1.194	20	127.6
7 0 1	1.185	0.001	1.184	20	54.7
6 1 2			1.183		
3 3 3	1.171	0.001	1.170	30	
5 5 1			1.173		67.85
7 1 1			1.173		
6 4 1	1.152	0.001	1.152	15	134.4
6 2 2			1.151		
7 2 1			1.142		
5 4 2	1.142	0.001	1.142	10	70.7
6 3 2			1.103		
4 3 3	1.102	0.001	1.101	5	37.1
5 0 3					
5 1 3	1.092	0.001	1.093	5	12.3
0 0 4	1.0735	0.0009	1.0763	10	99.9
5 5 2	1.0602	0.0008	1.0604	15	134.6
7 1 2					
8 2 0	1.0451	0.0007	1.0457	20	197.16
8 0 1			1.0455		
6 4 2			1.0447		
8 1 1	1.0374	0.0007	1.0379	10	163.4
7 4 1			1.0371		
7 2 2					
6 6 0	1.0153	0.0006	1.0162	20	60.0
8 2 1			1.0160		
6 1 3	1.0066	0.0006	1.0073	10	35.2
7 3 2	1.0016	0.0005	1.0015	15	78.3
6 6 1	0.9889	0.0004	0.9889	5	35.9

$^*I_{obs} = I/I_d = 2.033$ A ; values from densitometer chart.

$^\dagger I_{calc} = p|F|^2 \times 10^{-5}$; values of all $h\,k\,l$, which contribute to one diffraction line are added up.

Because of the fact than only the height of peaks (and not their area) was used and the Debye – and LP – factors were neglected, some discrepancies exist between F_{obs} and F_{calc} at higher angles θ.

References

1. L. A. DAVIS, R. RAY, C. P. CHOU and R. C. O'HANDLY, *Scripta Met.* **10** (1976) 541.
2. J. L. WALTER, J. F. BARTRAM, and R. R. RUSSELL, *Met. Trans. A* 9A (1978) 803.
3. H. CHANG and S. SASTRI, *ibid* 8A (1977) 1063.
4. J. L. WALTER, J. F. BARTRAM and I. MELLAS, *Mat. Sci. Eng.* **36** (1978) 193.
5. E. VAFACI-MAKHSOOS, E. L. THOMAS and L. E. TOTH, *Met. Trans. A* 9A (1978) 1449.
6. J. L. WALTER, P. RAO, E. F. KOCH and J. F. BARTRAM, *ibid* 8A (1977) 1141.

7. M. VON HEIMENDAHL and G. MAUSSNER, *J. Mater. Sci.* **14** (1979) 1238.

8. M. STUBIČAR, E. BABI, D. SUBASIČ, D. PAVUNA and Ž. MAROHNIČ *Phys. Stat. Sol. (a)* **44** (1977) 339.

9. R. E. MARINGER and C. E. MOBLEY, *J. Vac. Sci. Technol.* **11** (1977) 1067.

10. O. T. INAL and L. E. MURR, *J. Appl. Phys.* **49** (1978) 2427.

11. F. M. NORMAN, HENRY and KATHLEEN LOUDSDALE, "International Tables for X-ray Crystallography" Vol. 1 (Kynoch Press, Birmingham, 1952).

12. S. RUNDQVIST, *Acta Chem. Scand.* **16** (1962) 1.

13. E. W. MULLER and T. T. TSONG, "Field Ion Microscopy, Principles and Applications", (American Elsevier, New York, 1969) p. 206.

14. H. T. EVANS, D. E. APPLEMAN and D. S. HANDWERKER. Annual Meeting of the American Crystallography Association, Cambridge, Mass, 28 March 1963 (American Crystallography Association, Cambridge, Mass., 1963) p. 42.